Journal of Management and Sustainability; Vol. 13, No. 1; 2023
ISSN 1925-4725 E-ISSN 1925-4733
Published by Canadian Center of Science and Education

Characteristic Curves in Erodible Soils on a Slope in Cabo De Santo Agostinho/Brazil

Kalinny Patricia Vaz Lafayette[1], Roberto Q. Coutinho[2], José Ramon Barros Cantalice[3], Thiago Augusto da Silva[2], Amauri Gouveia Pessoa Neto[1], Luciana Cássia Lima da Silva[1] & Rayane Gabriella Pereira da Silva[1]

[1] University of Pernambuco - UPE, Recife, Brazil

[2] Federal University of Pernambuco - UFPE, Recife, Brazil

[3] Rural Federal University of Pernambuco - UFRPE, Recife, Brazil

Correspondence: R. Benfica, 455, 50720-001, Escola Politécnica de Pernambuco da Universidade de Pernambuco, PEC, Madalena, Recife, Brasil.

Received: March 10, 2023 Accepted: April 26, 2023 Online Published: May 3, 2023

doi:10.5539/jms.v13n1p201 URL: https://doi.org/10.5539/jms.v13n1p201

Abstract

Several studies focus on the characteristic curve of the soil, which plays a fundamental role in the mechanics of unsaturated soils and is also an important indicator of the physical quality. Therefore, the objective of this research was to determine the characteristic curve of the soil by the methods of Filter Paper, Richards Pressure Chamber, and Haines Funnel on an erodible slope in the Metropolitan Region of Recife, in the state of Pernambuco, Brazil. The curves were designed by the models of van Genuchten, Fredlund & Xing, Seki, and Dunner. In the suction x humidity ratios, during the wetting and drying processes, the experimental points were very close, making it difficult to define the hysteresis effect. The Richards Chamber and Haines Funnel methods allowed the complementation of the characteristic curve for low suction values, indicating that the techniques can be used simultaneously. The statistical analysis resulted in a numerical model with a significance value greater than 97%.

Keywords: characteristic curves, erodible soil, mathematical adjustments

1. Introduction

The knowledge of the behavior of the characteristic curve for unsaturated soil has been an important artifice for the analysis of the performance of its physical-hydric properties. It is also fundamental for several areas such as geotechnics, agriculture, hydrology, irrigation and fertilizer management, remediation of polluted areas, and many others, Silva, Libardi and Gimenes (2018); Ahmed et al. (2021); Yan, Birle and Cudmani (2021); Wang et al. (2021), in addition to its essential role in formulating constitutive equations applicable to unsaturated soils (Maranha Das Neves, 2016).

The soil-water characteristic curve (SWCC) is the relationship between water content (gravimetric or volumetric) or degree of saturation with suction (matrix or total) (FREDLUND et al., 2012). It is commonly illustrated in the semi-log space of volumetric water content and matric suction (θ:logψ) and contains fundamental information to describe geotechnical problems related to unsaturated soils (Rajesh et al., 2017).

As in the distribution of pores in the soil, it is possible to obtain dependence relationships between the coefficients of the mathematical equations that describe the characteristic curve and various soil properties, Cassáro et al. (2008). The presentation of the characteristic curve is influenced by properties such as structure and aggregation, initial moisture content, void index, soil type, nature and compaction energy, stress history, percentage of fines, mineralogy, pore size distribution, Parahyba et al. (2019), which may vary for each type of soil. The choice of the number of points used to determine the curve is usually arbitrary, without a specific criterion.

With the shape of the curve, it is possible to identify the classification as uni, bi, or trimodal: if the soil has only one pore size range (macro, meso, or micro), it is called unimodal. This strip can be narrow, characterizing uniform sand, or wide, characterizing well-graded sand. A soil that has two predominant bands can be considered bimodal. The trimodal distribution is considered less frequent (Oliveira, 2019).

Several laboratory types of equipment have been developed to obtain the characteristic curve independently, although in some cases obtaining the curve is an expensive, time-consuming, and complex process. Some researchers used the Tensiometer Method (Marinho et al., 2008), Pressure device (Bechtold et al., 2018), electrical resistance blocks (Zeitoun et al., 2021), and filter paper (Fattah et al., 2021).

In recent decades, many empirical models have been developed to predict the characteristic, such as Van-Genuechten (1980), Brooks-Corey (1964), Fredlund and Xing (1994), Gardner (1958), etc., and researchers have also compared and evaluated the applicability and consistency of other models (Matlan et al., 2015; Fattan et al., 2021). Based on this, scholars have investigated the characteristic curves of clay (Li et al., 2017), sand (Yan & Zhang, 2015) and expansive soil (Tamer et al., 2017; Ahmed et al., 2018), and analyzed the effect of dry density (Gallage & Uchimura, 2010), void ratios (Heshmati & Motahari, 2015), and grain size distribution on the curve (Chen et al., 2018; Zhai et al., 2020).

In the laboratory, undisturbed samples measure the sensitivity of matrix suction, particularly for relatively low suction values, in which capillary mechanisms tend to dominate the behavior of soil water retention.

Thus, to obtain the parameters of the characteristic curve, the methods of filter paper, Richards chamber, and Haines funnel were used to measure the matrix potential of water in samples of erodible soil on a slope located in the Metropolitan area of Recife/Brazil.

2. Method

2.1 Characterization of the Study Area

The area selected for the study is located on a hillside in the Armando de Holanda Cavalcanti Metropolitan Park, located in the municipality of Cabo de Santo Agostinho, in the southern portion of the Metropolitan Region of Recife, approximately 40 km from the capital. It occupies an area of approximately 270 ha. (total park surface), as shown in Figure 1. The choice of this area is associated with the alarming proportions of erosive features; the landscape presents intense gullies and ravines.

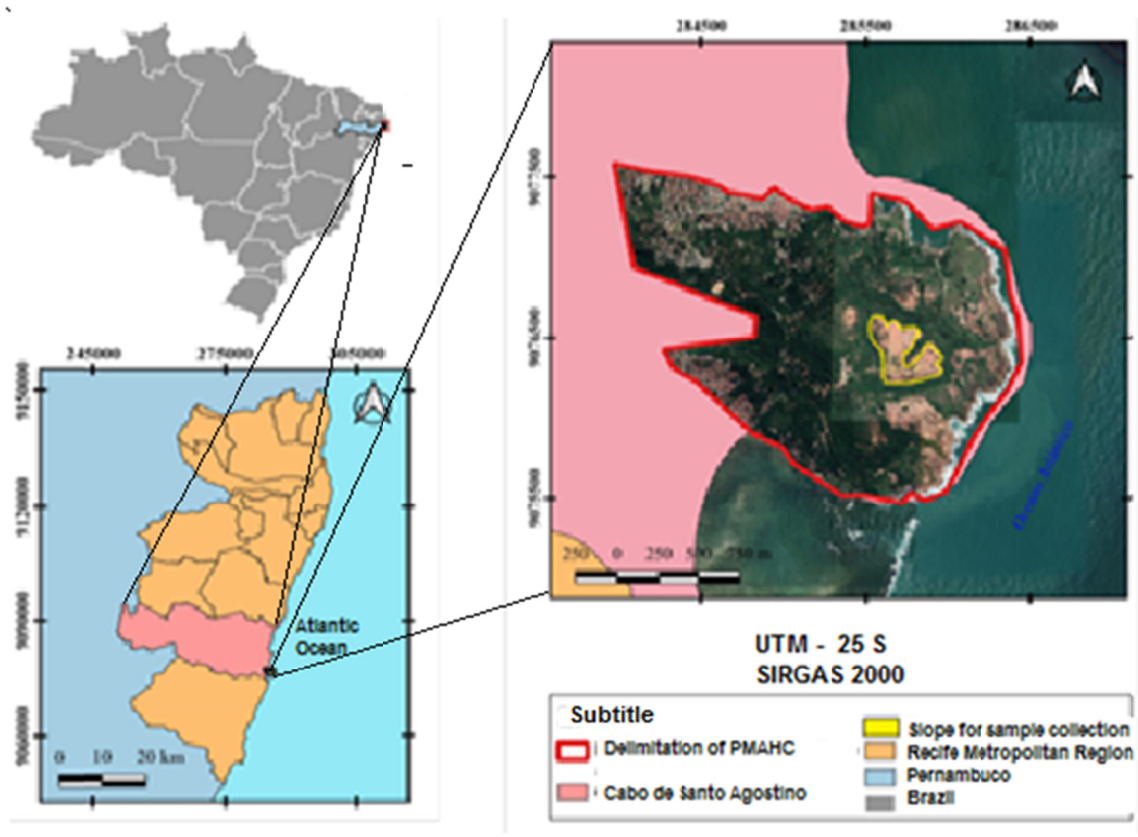

Figure 1. Location of the study area

2.2 Simple Recognition Poll

Three percussion-sounding holes were drilled on the central slope until the impenetrability condition was reached. In Figure 2, the penetration resistance index (SPT) values are practically constant along the profile, with the lowest value of 15 blows at 4.2 m depth, and the highest value of 60 blows at 15 m depth. depth.

The profile consists of a layer of clayey sand, followed by a 1.0 m thick silty sand and up to 4.3 m deep, clayey sand (5YR 7/3 – MUNSSEL, 1992), and up to this depth; the soil was identified as belonging to the Barreiras Formation.

This Formation has brightly colored tones that vary from yellow-red to white, outcropping on the eroded cliffs along the beaches and the steep slopes of the valleys. From this point on, there is a hard sandy clay (10YR 7/6 MUNSSEL, 1992), belonging to the residual granite soil, often marked by variation between light yellow and whitish veins (feldspars in alteration processes), referring to the passage of water and the removal of iron sesquioxides.

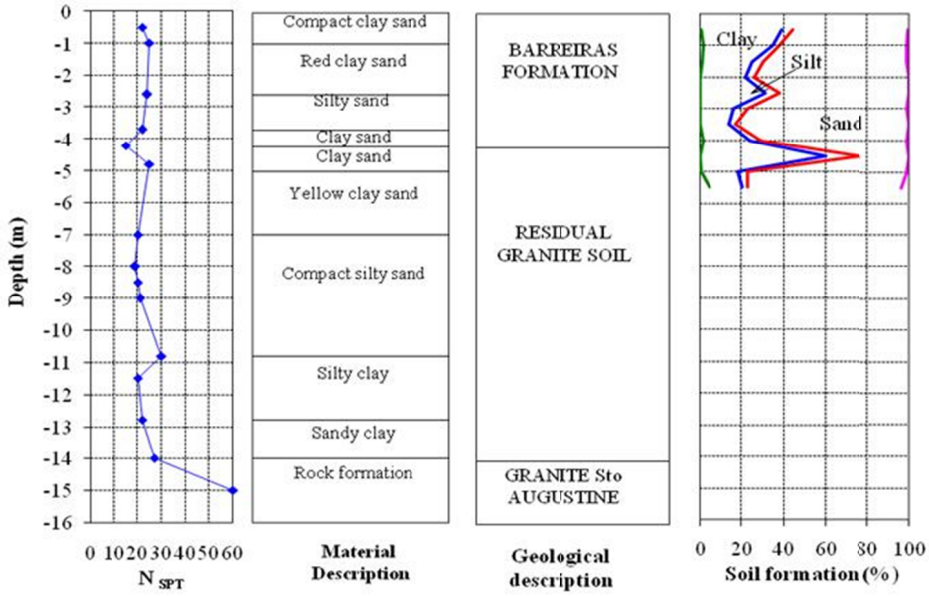

Figure 2. Location of the study area

2.3 Laboratory Geotechnical Investigation

Assays of physical and mineralogical characterizations were carried out and the characteristic curves were obtained by the filter paper, Haines, and Richards Pressure Chamber methods.

2.3.1 Physical Characterization

Soil granulometric analysis was performed every 0.5m depth reaching 5.5m depth, as shown in Table 1. Soils were classified from loamy sand to sandy clay. Geologically, it is assumed that there are two distinct types of soil formation in the profile: soil belonging to the Barreiras Formation up to a depth of 4.5 m and, from this depth, residual granite soil.

Table 1. Grain size composition

Features	1,5 m–1,8 m (FB)*	4,5 m–4,8 m (SR)*
Clay	25	60
Silt	5	16
Sand	69	24
Boulder	1	-
IP	9,5	22

Note. *FB – the soil of the Barreiras Formation; *SR – residual granite soil.

2.4 Mineralogical Analysis

The analysis of soil microstructure in systems susceptible to erosion can help a lot in understanding certain behaviors and in finding solutions. The first would deal with the explanation of the behavior and functioning, as the systems are, and the second would deal more with the search for desirable patterns of microstructures, which could guarantee a longer useful life for engineering control works, or soil conservation. For the time being, microstructures have served as an important aid in understanding the behavior and functioning of soil systems and as a strong ally of other indicators used for a long time in erosion studies. Soil microstructure analysis was performed using scanning electron microscopy (SEM). In Figure 3 (a, b) the soil structure is characterized by quartz grains, which are partially or covered with fine material (clay and iron oxide). It is a potentially thin matrix with poorly selected grains (subrounded and rounded). Some simple packings are identified where the grains are directly connected. For Earle (2019), quartz represents a non-reactive material and is quite resistant to weathering, providing greater stability to the soil structure.

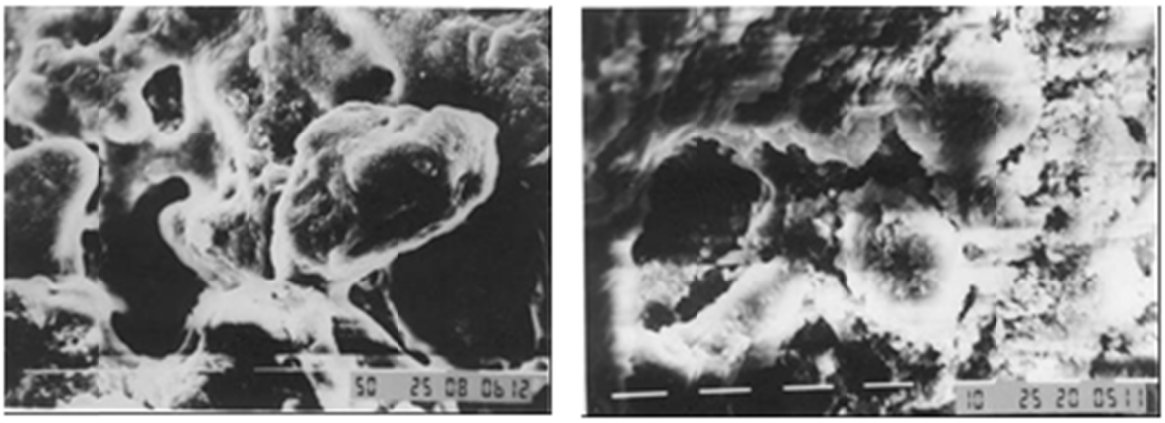

Figure 3. Scanning electron microscopy. a) (1.5 m - 800X magnification); b) (4.5 m - 1000X magnification)

Mineralogy using the petrographic microscope confirmed the presence of quartz, biotite, and muscovite and identified minerals such as plagioclase (the mineral from the sodium feldspar group) and orthoclase (the mineral from the potassium feldspar group), as shown in Figures 4, respectively. The images had a magnification of 100X and are with crossed-Nicols, that is, two polarizers that let through rays that are vibrating orthogonally to each other; the polarizer and the microscope analyzer are at 90º. Figure 4 was visualized with an auxiliary slide so that the minerals could be identified through the colors. The orange and blue colors represent quartz, purple orthoclase, brown biotite, and reddish purple represent plagioclase.

As for the Santo Agostinho granite, it corresponds to the surface with the largest outcrop area. Predominant equigranular rocks, medium to coarse texture and whitish gray to pink color. The essential mineralogy is represented by feldspar, orthoclase, plagioclase, and quartz, making up more than 90% of the set of minerals, while the mafic phases vary between 0.4 and 10%.

Feldspar makes up the group of primary minerals, being among the most common in rocks and the earth's crust itself, being also relatively resistant to weathering (Saraiva et al., 2020). It is found most often in the sand and silt fractions and, only in small amounts, in clay, so its presence depends on the composition of the parent rock and the intensity of weathering to which it has been exposed (Earle, 2019).

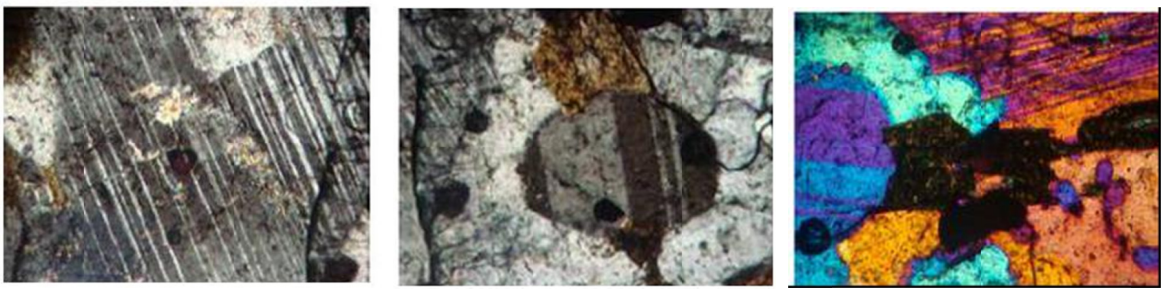

Figure 4. Plagioclase, orthoclase and quartz, orthoclase and biotite

The main mafic mineral is amphibole, Figure 5, which can reach up to 4.1%, still occurring as opaque accessories. In orthoclasses, subhedral grains up to 0.5 mm and is frequently serialized to varying degrees. Figure 5 presents granophyric texture, represented mainly by radial and spherulitic fringe types. This is a texture formed by the simultaneous intergrowth of quartz, which together with the cavities seen in the field, confirm the hypabyssal positioning.

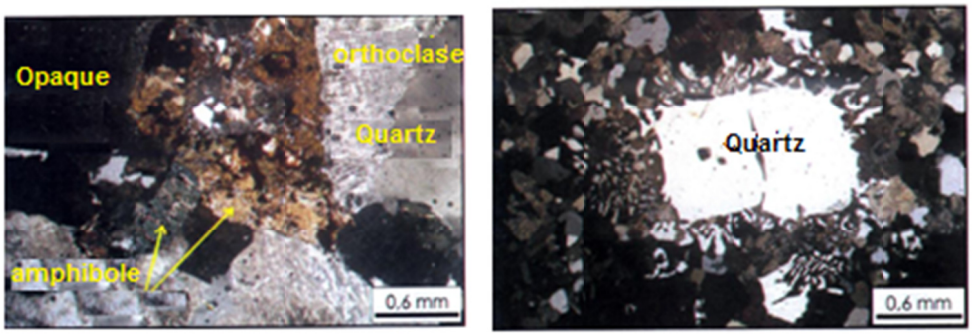

Figure 5. Microscopic features of the Granite in Santo Agostinho (Nascimento, 2003).

2.5 Characteristic Curves

The soil water characteristic curve shows the relationship between soil water and water potential providing information to quantify and model soil water processes for groundwater input, storage, flow, and recharge. It can be obtained through traditional direct or indirect methods.

Direct methods result in suction measurements without the need for correlations between this and other soil parameters. Indirect methods allow the determination of soil suction through its relationship with the properties of other materials. Therefore, choosing the best method depends on the time for carrying out the tests and the equipment.

Several empirical models have been proposed and used to describe the curve from a certain number of measured points. These empirical functions are still widely used to adjust soil characteristic curves. Thus, important experimental research has enabled the determination of parameters in the characteristic curves: Lafayette (2006); Carvalho et al. (2015); Zeitoun et al. (2021); Li and Vanapalli (2021). In this research, the characteristic curves of the soils were obtained by the Filter Paper methods, suction lacquer or Haines funnel, and pressure plate or Richard Chamber. The curves were calculated according to the models of Van Genutchen (1980); Fredlung and Xing (1994), Dunner (1994) e Seki (2007).

2.5.1 Filter Paper

In determining the suction values of the water retention curve, the filter paper technique was applied, considering the different advantages it presents and its diffusion in the academic environment (Marinho & Oliveira, 2006; Lafayette, 2006; Campos, 2015; Trevisolli, 2018; Hernandez, 2020; Wang et al., 2021; Zhou et al., 2021).

The filter paper method consists of indirect quantification through filter papers and matrix or total soil suction (Carvalho et al., 2015). The filter paper used was Whatman No. 42 type 2. To determine the matrix suction, the

undisturbed samples were molded into metallic rings measuring 7.20 cm in diameter and 3.0 cm in height. The equilibrium time used was approximately 7 days. After equilibrium, soil and filter paper moisture is obtained. Suction is achieved through the calibration curve of the filter paper through its humidity. Figure 6 shows the samples with the filter paper.

Figure 6. Test execution with filter paper

2.5.2 Haines Funnel

The Haines Method is used to determine the soil suction, only for low-stress points on the curve. The equipment is composed of a porous plate properly saturated, a flexible tube connected to a compartment filled with water, and a level regulator. The porous plate also called the suction plate, must have an air inlet value of less than 40 kPa, Carvalho et al. (2015). Porous plates with very high air inlet values, above 70 kPa, can cause very time-consuming tests, due to the low permeability of the porous material.

The samples were molded into PVC rings, with a diameter of 5.2 cm and a height of 2.5 cm and placed on the porous plates of the funnels. Then water was added until saturation, around 24 h. Suctions were applied: 0.1 kPa; 0.3 kPa; 0.5 kPa; 1.0 kPa; 1.5 kPa; 2.0 kPa; 3.0 kPa; 5.0 kPa; 7.5 kPa and 10 kPa. Figure 7 illustrates carrying out the test.

Figure 7. Test execution (Meurer, 2014)

2.5.3 Richards Pressure Chamber

The pressure plate apparatus allows the direct measurement of water content under matrix suction applied to a sample and used to withstand high pressures Hong et al. (2016).

This equipment, Figure 8, allows the extraction of soil moisture, through the drying process with a pressure of 1500 kPa. The ceramic plate has its underside covered by a rubber diaphragm sealed at its edge. Between the plate and the diaphragm, there is a nylon screen that allows the solution to flow during the application of pressure. It causes the solution to move from the ground to the small reservoir under the plate, dripping in the outlet tube.

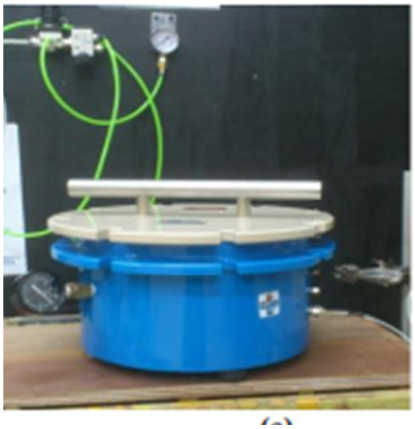

Figure 8. Pressure chamber by Richards Azmi et al. (2019)

Four undisturbed samples were molded in PVC rings, with a diameter of 5 cm and a height of 1 cm and taken to the Richards Pressure Chamber, where the applied suctions were: 10.33 kPa; 34 kPa; 53.7 kPa; 258 kPa; 775 kPa and 1549 kPa.

At the break-even point (typically 10 days after the start of the test), the applied suction was turned off and each ring was weighed. Then the samples were taken to the oven to determine their humidity.

2.5.4 Response Surface Methodology

The response surface methodology (RSM) is a mathematical and statistical method widely used for modeling and analyzing a process in which the response of interest is influenced by multiple variables. The objective is to optimize the response. The parameters that affect the process are called dependent variables.

Thus, for the solution, an empirical mathematical model is necessary, as the RSM needs to establish the relationship between the independent variables and the response variables. Therefore, the adequacy of the problem can be assessed for linear functions of the first order, quadratics of the second order, or polynomials of the higher order (Olgun, 2013).

The model used in the research was based on the general form of the complete quadratic model presented by Güllü and Fedakar (2017), as presented in Equation 1:

$$RCS = b_0 + \sum b_i X_i + \sum b_j X_j + \sum b_k X_k + \sum b_{ii} {X_i}^2 \quad (1)$$

Where the terms X_i and b represent the i-th random variable and the coefficients of the complete quadratic model, respectively.

From the determination of the quadratic model, it is necessary to verify its adherence, which takes place through the externalized conference of the residuals, with the conference by possible outliers, and with the calculation of the coefficients of determination (R^2), Adjusted R^2, and the predicted R^2.

The model verification formulations are presented in Equations 2 to 4, according to the model proposed by Güllü and Fedakar (2017).

$$R^2 = \frac{SSR}{SSM+SSR} \quad (2)$$

Where *SSR* and *SSM* are the sum of the squares of the residuals and the model, respectively. The sum of both parameters produces the *SST* coefficient (sum of total squares).

$$R^2 Adjusted = 1 - \frac{n-1}{n-p}(1 - R^2) \quad (3)$$

Where *n* and *p* are, respectively, the number of observations and the model parameters containing intercepts.

$$R^2 Predicted = 1 - \frac{PRESS}{SST} \quad (4)$$

Where PRESS is the error of the predicted sum of squares. This coefficient is obtained through the difference

between the actual or measured and predicted values, that is, the residual sum of squares.

The general form of the independent variables used in the complete quadratic model was identified based on the analysis of the parameters obtained with the parameters of the soil characteristic curve. The entire analysis was performed with the help of Minitab Statistical Software (version 19.0), which made it possible to apply the RSM method, as well as the ANOVA analysis.

3. Results and Discussion

The characteristic curve is an important relationship to interpreting the response of unsaturated soil. It represents how the permeability, the shear strength, and the volumetric deformations behave under the variation of suction, obtained through wetting paths and drying. Table 2 presents the initial conditions of each specimen, the gravimetric (w_s), and volumetric (θ_s) mixtures.

Table 2. Physical indices of samples for determination of characteristic curves

Depth (m)	w_o (%)	γ_o (kN/m^3)	e_o	S_o (%)	Saturation Humidity	
					Ws (%)	θ_s (%)
P 01 (1,5)	12,97	14,30	0,83	40,86	31,67	45,33
	12,89	14,51	0,81	41,95	30,92	44,75
P 01 (4,5)	11,46	13,97	0,90	33,81	33,96	47,36
	11,69	13,90	0,91	34,20	34,33	47,64

The characteristic curves of the soils obtained through the filter paper, Haines funnel, and Richards chamber methods are in Figures 11 and 12. The points of the curves during the wetting and drying process were very close, making it difficult to identify the effect of hysteresis. Different hypotheses have been formulated to explain the hysteresis of the characteristic curves; however, the best bases on differences in pore sizes, in which large and small pores are interconnected, both during drying and wetting. This process can be interrupted by the pores influencing the suction values.

The characteristic curve was transformed concerning the void ratio to facilitate the analysis of tropical soils since it considers the pore size, which is generally not homogeneous. In this case, at each point on the curve, the measurements in pF are multiplied by the respective void indices, removing its influence on the characteristic curve. The soils at Point P-01 (1,5m), Figure 9, present an air entry value of around 1.5 kPa, where desaturation of the soil macrostructure begins. This initial desaturation occurs for low suctions down to plus or minus 10kPa. For Figure 10 at Point P-01 (4,5m) in residual granite soil, the characteristic curves are typical of clayey soils, presenting a non-homogeneous (bimodal) pore distribution. This distribution is due to weathering, which is responsible for the formation of aggregation of cemented particles or clay bridges. The shapes of the curves are similar to a “saddle” and can be divided into three distinct sections. The sample has a first air entry value (in the macropores) for small suctions, around 4 kPa, where desaturation begins. Afterward, a practically horizontal level is observed, with the suction varying from 100 kPa to 2200 kPa. This threshold makes it hard to interpret residual suction as a single value. In the last stretch, the second air entry value occurs, where the moisture content decreases again with the addition of suction due to water removal in the soil microstructure.

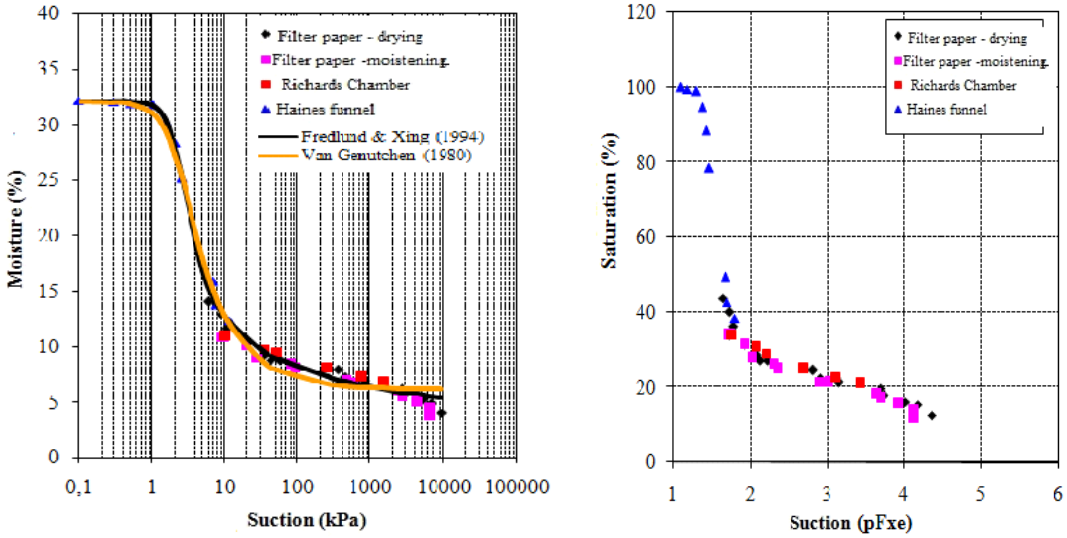

Figure 9. Characteristic curve – 1,5m

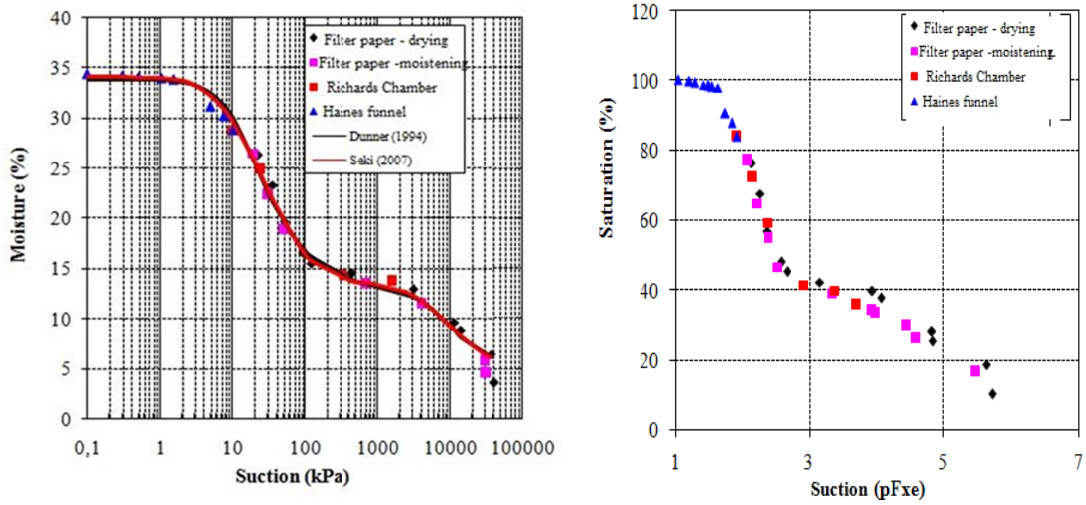

Figure 10. Characteristic curve – 4,5m

Table 3 presents the results of the statistical adjustments (R2) performed based on the equations of Fredlund and Xing (1994) and Van Genutchen (1980), Dunner (1994), and Seki (2007).

It is observed that for the clayey sand at point P-01 (1.5m), the model that best fitted was the one by Fredlung and Xing (1994) with (R^2 = 0.998); as for the sandy clay P -01 (4.5m), the fit that had the highest (R2 = 0.995) was the Seki model (2007).

Table 3. Parameter result (R2)

Points	P 01(FB) -1,5m		P 01(SR) - 4,5m	
Parameters	VAN GENUTCHEN (1980)	FREDLUND e XING (1994)	DUNNER (1994)	SEKI (2007)
R^2	0,994	0,998	0,994	0,995

3.1 Statistical Analysis

In order to obtain a full glimpse of the soil suction behaviour, statistical modeling was performed to measure the importance that each statistical factor has on the variation of the soil suction. The range of values of the

independent factors used in this study are listed in Table 4.

Table 4. Independent factors and their range

Term	Range
Pfx e (Pe)	1.04 to 7.72
Saturation (SAT)	10.34% to 100%

According to Myers, Montgomery e Anderson-Cook (2009); Güllü e Fedakar (2017), and Silva et al. (2021) to assure the success of the statistical model, the confiability of the measured factors is essencial. In order to provide a higher rate of accuracy in the resulting model, it was necessary to suppress some of the outliers witthin the independent factors and also of some of the factor interactions (SAT*SAT). Table 5 shows all of the independent factors and the interactions used to create the full-quadratic model.

Table 5. Analysis of variance

Source	Degrees of freedom	Adj SS	Adj MS	F-Value	P-Value
Model	4	4079678608	1019919652	179.17	0.000
Linear	2	2473911743	1236955871	217.30	0.000
Pe	1	65692397	65692397	11.54	0.002
SAT	1	6890	6890	0.00	0.043
Square	1	154278908	154278908	27.10	0.000
Pe*Pe	1	154278908	154278908	27.10	0.000
2-Way Interaction	1	29504706	29504706	5.18	0.032
Pe*SAT	1	29504706	29504706	5.18	0.032
Error	25	142310223	5692409		
Total	29	4221988831			

The results of the interactions show good fitting for the model behavior, especially for the factors Pe and Pe*Pe, who presented values very close to zero for the P-Values. According to Shirazi, Khademalrasoul e Ardebili (2020) and Silva et al. (2021) those results are way below the limit for the P-Values (0.05) for RSM studies involving soil parameters, indicating that the independent factors involving Pe have a strong influence on the soil suction results.

The regression values obtained for the modeling were sumarized on Table 6. The results showed excellent confiability values for R^2 (96.64%), which according to Myers Montgomery e Anderson-Cook (2009) and Silva et al. (2021) is a good parameter to evaluate how the model can represent accurately the behavior of a soil geotechnical property. The other regression results were 95,94% and 93,82% for the Adjusted R^2 and the Predicted R^2, respectively, showing a difference of less than 20% between the R^2 values as it is recommended by DeLoach e Ulbrich (2007).

Table 6. Sumarized regression values

S	**R^2 (Model)** *R-sq*	**R^2 Adjusted)** *R-sq(adj)*	**R^2 Predicted** *R-sq(pred)*
38,1015	97.76%	96.80%	94.94%

With the excellent values obtained for the regression analysis (Table 6), the model is now considered valid and can be used for optimization purposes. The quadratic polynomial equation suggested through the RSM methodology is now presented in equation 5.

$$SUCTION = 86078 - 48096 \cdot Pe - 55317 \cdot SAT + 6738 \cdot Pe \cdot Pe + 16257 \cdot Pe \cdot SAT \quad (5)$$

After the model validation, it was possible to draw the response surface, which is a key aspect of any RSM analysis, making it possible to easily visualize which corresponding regions of the surfaces indicate response minimization or maximization (Figure 11).

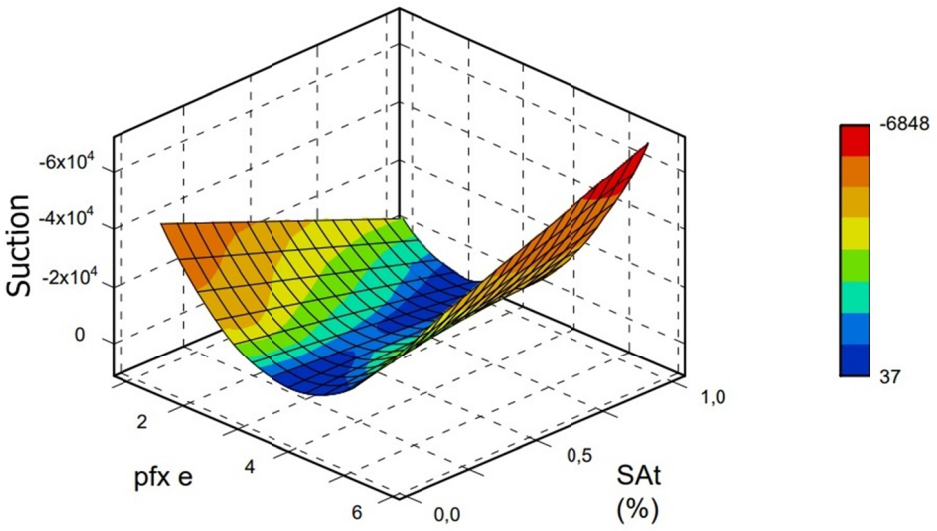

Figure 11. Quadratic model response surface

The surface and model analysis showed that the mean interactions of the model showed the overall model-tendency for reducing the value of the soil suction, leading the present study to optimize the model response for the minimization of the soil suction. Therefore several conditions were applied to the model to restrict the higher volume of mean results of possible suction solutions, leading to the interaction result presented in Table 7.

Table 7. Predicted values for the optimized (minimized) response of the model

Variable	*Setting*
Pe	2.36482
SAT	100%
SUCTION	-6868.47

The selected values for the independent variables (Pe and SAT), show the lowest possible value for soil suction, using the selected data. The overall behavior of the variable Pe shows that the suction results tend to decrease until certain value (2.36482) and then tend to increase rapidly This relationship between soil suction and Pefapproaches the shape of a parable with downward concavity, i.e., with a defined minimum point.

As for the variable SAT, the results show that by increasing its values, the suction response tends to decrease. That behavior indicates a negative variation (decreasing in value) as the SAT variable increase in value, almost assuming a negative linear relationship.

4. Conclusion

For evaluating characteristic curves, filter paper, Richards chamber, and Haines funnel methods were used, considering efficient and complementary mainly to obtain low suction values.

Adjustments were used according to the models of Van Genutchen (1980); Fredlung and Xing (1994) for sandy-clay soil at 1.5m depth. A bimodal tendency of pore distribution was identified in the characteristic curve of the clayey-sandy soil, indicating that the microstructure and macrostructure command the entry and exit of water from the pores of the soil, with the proposed adjustment by Dunner (1994) and Seki (2007). The models were considered adequate concerning the experimental data, with an R2 above 99%.

The statistical optimization analysis resulted in a numerical model with an $R^2 = 97.76\%$. Finally, tendency of the suction results to decrease, as long as the SAT values increased, to a certain point and then increasing behavior for the independent variable Pe.

References

Ahmed, A., Alam, J. B., Pandey, P., & Hossain, S. (2021). Estimation of Unsaturated Flow Parameters and Hysteresis Curve from Field Instrumentation. *Web Of Conferences*, *337*, 01008.

https://doi.org/10.1051/matecconf/202133701008

Ahmed, M. A., Tamer, Y. E., & Mosleh, A. A. (2018). Hysteresis Soil-Water Characteristic Curves of Highly Expansive Clay. *European Journal of Environmental and Civil Engineering*, *22*(9), 1041–1059. https://doi.org/10.1080/19648189.2016.1229232

Azmi, M., Ramli, M. H., Hezmi, M. A., Mohd Yusoff, S. A. N., & Alel, M. N. A. (2019). *Estimation of Soil Water Characteristic Curves (Swcc) Ofmining Sand Using Soil Suction Modelling*. Materials Science and Engineering Publishing. https://doi.org/10.1088/1757-899X/527/1/012016

Bechtold, M., Dettmann, U., Wöhl, L., Durner, W., Piayda, A., & Tiemeyer, B. (2018). Comparing Methods for Measuring Water Retention of Peat Near Permanent Wilting Point. *Soil Sci. Soc. America J.*, *82*, 601–605. https://doi.org/10.2136/sssaj2017.10.0372

Brooks, R., & Corey, A. (1964). *Hydraulic Properties of Porous Media*. Hydrology Paper. Fort Collins, Colorado: Colorado State University.

Campos, L. G. (2015). *Variação Da Resistividade Elétrica Para Três Solos Não Saturados*. Universidade Estadual Paulista Julio Mesquita Filho.

Carvalho, J. C. D. et al. (2015). *Solos Não Saturados No Contexto Geotécnico*.

Cassáro, F. A. M., Pires, L., Santos, F. R. A., Gimenez, D., & Reichardt, K. (2008). Funil De Haines Modificado: Curvas De Retenção De Solos Próximos À Saturação. *R. Bras. Ci. Solo*, *32*, 2555–2562. https://doi.org/10.1590/S0100-06832008000600032

Chen, X., Hu, K., Chen, J., & Zhao, W. (2018). Laboratory Investigation of the Effect of Initial Dry Density and Grain Size Distribution on Soil-Water Characteristic Curves of Wide-Grading Gravelly Soil. *Geotech Geol. Eng.*, *36*, 885–896. https://doi.org/10.1007/s10706-017-0362-1

Deloach, R., & Ulbrich, N. A. (2007). Comparison of Two Balance Calibration Model Building Methods. *American Institute of Aeronautics and Astronautics*, *1*, 1–81. https://doi.org/10.2514/6.2007-147

Dunner, W. (1994). Hydraulic Conductivity Estimation for Soils with Heterogeneous Pore Structure. *Water Resourses Res.*, *30*, 211–223. https://doi.org/10.1029/93WR02676

Earle, S. (2019). *Physical Geology* (2nd ed.). Victoria, B.C.: Bc Campus. Retrieved from Https://Opentextbc.Ca/Physicalgeology2ed/.Acesso Em: 01set. 2021.

Fattah, M. Y., Majeed, Q. G., & Joni, H. H. (2021). Comparison Between Methods of Soil Saturation on Determination of the Soil Water Characteristic Curve of Cohesive Soils. *Arab J. Geosci.*, *14*, 1–10. https://doi.org/10.1007/s12517-020-06362-y

Fredlund, D. G., & Xing, A. (1994). Equations for the Soil-Watercharacteristic Curve. *Canadian Geotechnical Journal*, *31*, 521–532. https://doi.org/10.1139/t94-061

Fredlund, D. G. H., & Rahardjo, M. D. F. (2012). *Unsaturated Soil Mechanics in Engineering Practice* (2nd ed.). Hoboken, Nj: Wiley. https://doi.org/10.1002/9781118280492

Gallage, C. P. K., & Uchimura, T. (2010). Effects of Dry Density and Grain Size Distribution on Soil-Water Characteristic Curves of Sandy Soils. *Soils And Foundations*, *50*, 161–172. https://doi.org/10.3208/sandf.50.161

Gardner, W. R. (1958a). *Mathematics of Isothermal Water Conduction in Unsaturated Soil* (pp. 78–87). Highway Research Board Special Report, Washington.

Gardner, W. R. (1958b). Some Steady State Solutions of the Unsaturated Moisture Flow Equation with Application to Evaporation from a Water Table. *Soil Science*, *85*, 228–232. https://doi.org/10.1097/00010694-195804000-00006

Güllü, H., & Fedakar, H. I. (2017). Response Surface Methodology for Optimization of Stabilizer Dosage Rates of Marginal Sand Stabilized with Sludge Ash and Fiber Based on Ucs Performances. *Ksce Journal of Civil Engineering*, *21*(5), 1717–1727. https://doi.org/10.1007/s12205-016-0724-x

Hernandez, Y. M. R. (2020). *Influência Da Sazonalidade Climética Na Estabilidade De Talude Em Voçorocas No Complexo Metamórfico Do Bação* (p. 129). Dissertação (Mestrado Acadêmico). Universidade Federal De Ouro Preto. Núcleo De Geotecnia Da Escola De Minas. Programa De Pósgraduação Em Geotecnia.

Heshmati, A. A., & Motahari, M. R. (2015). Modeling the Dependency of Suction Stress Characteristic Curve on Void Ratio in Unsaturated Soils. *Ksce J. Civ Eng.*, *19*, 91–97. https://doi.org/10.1007/s12205-013-1185-0

Hong, W.-T., Jung, Y.-S., Kang, S., & Lee, J.-S. (2016). Estimation of Soil-Water Characteristic Curves in Multiple-Cycles Using Membrane and Tdr System. *Materials*, *9*. https://doi.org/10.3390/ma9121019

Lafayette, K. P. V. (2006). *Estudo Geológico-Geotécnico Do Processo Erosivo Em Encostas No Parque Metropolitano Armando De Holanda Cavalcanti-Cabo De Santo Agostinho/Pe* (p. 358). Programa De Pós-Graduação Em Engenharia Civil Tese De Doutorado. Universidade Federal De Pernambuco.

Li, J. H., Lu, Z., Guo, L. B., & Zhang, L. M. (2017). Experimental Study on Soilwater Characteristic Curve for Silty Clay with Desiccation Cracks. *Eng. Geology*, *218*, 70–76. https://doi.org/10.1016/j.enggeo.2017.01.004

Li, Y., & Vanapalli, S. K. (2021). A Novel Modeling Method for the Bimodal Soil-Water Characteristic Curve. *Computers and Geotechnics*, *138*, 1–15. https://doi.org/10.1016/j.compgeo.2021.104318

Maranha Das Neves, E. (2016). *Mecânica Dos Estados Críticos: Solossaturados E Não Saturados* (1st ed., p. 528). Lisboa, Ist Press.

Marinho, F. A. M., & Oliveira, O. M. (2006). The Filter Paper Method Revisited. *Geotechnical Testing Journal*, *29*(3), 250–258. https://doi.org/10.1520/GTJ14125

Marinho, F. A. M., Take, W. A., & Tarantino, A. (2008). Measurement of Matric Suction Using Tensiometric and Axis Translation Techniques. *Geotech Geol. Eng.*, *26*, 615–631. https://doi.org/10.1007/s10706-008-9201-8

Matlan, S. J., Taha, M. R., & Mukhlisin, M. (2015). Assessment of Model Consistency for Determination of Soil-Water Characteristic Curves. *Arab J. Sci. Eng.*, *41*, 1233–1240. https://doi.org/10.1007/s13369-015-1888-2

Munsell Color Company, Inc. (1992). *Munsell Soil Color Chort Baltmore/Maryland/, Usa*.

Myers, R. H., Montgomery, D. C., & Anderson-Cook, C. M. (2009). *Response Surface Methodology: Process and Product Optimization Using Designed Experiments* (3rd ed.). New Jersey, Usa: John Wiley&Sons.

Nascimento, M. A. L. (2003). *Gologia, Geocronologia, Geoquímica E Prtogênese Das Rochas Ígneas Cretáceas Da Província Magmática Do Cabo E Suas Relações Com As Unidades Sedimentares Da Bacia Pernambuco* (Ne Do Brasil, p. 233). Tese De Doutorado Ufrn.

Olgun, M. (2013). Effects of Polypropylene Fiber Inclusion on the Strength and Volume Change Characteristics of Cement-Fly Ash Stabilized Clay Soil. *Geosynthetics International*, *20*(4), 263–275. https://doi.org/10.1680/gein.13.00016

Oliveira, A. (2019). *Resistência E Compressibilidade De Solo Argiloso Tropical Residual Evoluído De Basalto/Maringá* (p. 191). Programa De Pós-Graduação Em Engenharia Civil Da Universidade Estadual De Maringá Pr.

Parahyba, R. B. V., Araújo, M. S. B., Almeida, B. G., Rolim Neto, F. C., Sampaio, E. V. S. B., & Caldas, A. M. (2019). *Water Retention Capacity in Arenosols and Ferralsols in A Semiarid Area in the State of Bahia, Brazil*. An Acad Bras Cienc. https://doi.org/10.1590/0001-3765201920181031

Rajesh, S., S. & Roy, S. M. (2017). Study of Measured and Fittedswcc Accounting the Irregularity in the Measured Dataset. *International Journal of Geotechnical Engineering*, *11*, 321–331. https://doi.org/10.1080/19386362.2016.1219541

Saraiva, S. M., Fraga, V. D. S., Araújo Filho, J. C. D., Santos, R. F. D., Felix, E. D. S., & Carneiro, K. A. A. (2020). Mineralogia De Luvissolos Formados Sob Gradiente Pluviométrico No Semiárido Paraibano. *Brazilian Journal of Animal and Environmental Research*, *3*(4), 4416–4433. https://doi.org/10.34188/bjaerv3n4-142

Seki, K. (2007). Swrc Fit – A Nonlinear Fitting Program with a Waterretention Curve for Soils Having Unimodal and Bimodal Porestructure. *Hydrology and Earth System Sciences Discussions*, *4*, 407–437. https://doi.org/10.5194/hessd-4-407-2007

Shirazi, M., Khademalrasoul, A., & Ardebili, S. M. S. (2020). Multi-Objective Optimization of Soil Erosion Parameters Using Response Surface Method (Rsm) in the Emamzadeh Watershed. *Acta Geophysica*, *68*(2), 505–517. https://doi.org/10.1007/s11600-020-00404-5

Silva Mln, L. P., & Gimenes, F. (2018). Soil Water Retention Curve as Affected by Sample Height. *Rev Bras Cienc Solo.*, *42*, E0180058. https://doi.org/10.1590/18069657rbcs20180058

Silva, T. A. D., Lafayette, K. P. V., Silva, L. C. L. D., Santos, M. J. P. D., & Bezerra, J. D. S. (2021).

Optimization of the Dosage of Sustainable Materials for the Stabilization of an Erosive Soil. *European Academic Research*, *9*.

Tamer, Y. E., Ahmed, M. A., Muawia, D., & Mosleh, A. A. (2017). Effect of Compaction State on the Soil Water Characteristic Curves of Sand-Natural Expansive Clay Mixtures. *Eur. J. Environ. Civil Eng.*, *21*, 289–302. https://doi.org/10.1080/19648189.2015.1112844

Trevizolli, M. N. B. (2018). *Proposta De Modelo Para Avaliação De Risco De Deslizamentos Baseado Em Cenários De Eventos Pluviométricos: Aplicação Em Um Talude Da Serra Do Mar No Trecho Pr/Sp. 197 F. Dissertação (Mestrado Em Geotecnia) - Setor De Tecnologia*. Universidade Federal Do Paraná, Curitiba.

Van Genuchten, M. T. (1980). A Closed-Form Equation for Predictingthe Hydraulic Conductivity of Unsaturated Soils. *Soil Sciencesociety of America Journal*, *44*, 892–898. https://doi.org/10.2136/sssaj1980.03615995004400050002x

Wang, Y., Li, T. L., Ping, L., Lei, Y., & Lawrence, D. D. (2021). Measurement and Uniform Formulation of Soil-Water Characteristic Curve for Compacted Loess Soil with Different Dry Densities. *Advances in Civil Engineering*, *2021*. https://doi.org/10.1155/2021/6689680

Yan, W., Birle, E., & Cudmani, R. (2021). *A Simple Approach for Predicting Soil Water Characteristic Curve of Clayey Soils Using Pore Size Distribution Data*. Matec Web of Conferences 337, Panam-Unsat 2021, 1-8. https://doi.org/10.1051/matecconf/202133702012

Yan, W. M., & Zhang, G. (2015). Soil-Water Characteristics of Compacted Sandy and Cemented Soils with and without Vegetation. *Can. Geotech. J.*, *52*, 1331–1344. https://doi.org/10.1139/cgj-2014-0334

Zeitoun, R., Vandergeest, M., Vasava, H. B., Machado, P. V. F., Jordan, S., Parkin, G., et al. (2021). In-Situ Estimation of Soil Water Retention Curve in Silt Loam and Loamy Sand Soils at Different Soil Depths. *Sensors*, *21*, 447–461. https://doi.org/10.3390/s21020447

Zhai, Q., Rahardjo, H., Satyanaga, A., & Dai, G. (2020). Estimation of the Soil-Water Characteristic Curve from the Grain Size Distribution of Coarse-Grained Soils. *Eng. Geology.*, *267*. https://doi.org/10.1016/j.enggeo.2020.105502

Zhou, J., Ren, J., & Li, Z. (2021). An Improved Prediction Method of Soil-Water Characteristic Curve by Geometrical Derivation and Empirical Equation. In *Hindawi Mathematical Problems in Engineering*. https://doi.org/10.1155/2021/9956824

Copyrights

Copyright for this article is retained by the author, with first publication rights granted to the journal.

This is an open-access article distributed under the terms and conditions of the Creative Commons Attribution license (http://creativecommons.org/licenses/by/4.0/).